RAPID COMMUNICATION

Filamentation instability in two counter-streaming laser plasmas

Hui Liu(刘慧)[1], Quan-Li Dong(董全力)[1,7,†], Da-Wei Yuan(袁大伟)[2,3], Xun Liu(刘勋)[2], Neng Hua(华能)[4], Zhan-Feng Qiao(乔战峰)[4], Bao-Qiang Zhu(朱宝强)[4], Jian-Qiang Zhu(朱健强)[4], Bo-Bin Jiang(蒋柏彬)[5], Kai Du(杜凯)[5], Yong-Jian Tang(唐永健)[5], Gang Zhao(赵刚)[3], Xiao-Hui Yuan(远晓辉)[6,7], Zheng-Ming Sheng(盛政明)[6,7,8], and Jie Zhang(张杰)[6,7]

[1] *School of Physics and Optoelectronic Engineerings, Ludong University, Yantai* 264025, *China*
[2] *Beijing National Laboratory of Condensed Matter Physics, Institute of Physics, Chinese Academy of Sciences, Beijing* 100190, *China*
[3] *National Astronomical Observatories of China, Chinese Academy of Sciences, Beijing* 100012, *China*
[4] *National Laboratory on High Power Lasers and Physics, Shanghai* 201800, *China*
[5] *Research Center of Laser Fusion, Chinese Academy of Engineering Physics, Mianyang* 621900, *China*
[6] *Department of Physics, Shanghai Jiao Tong University, Shanghai* 200240, *China*
[7] *Innovative Collaboration Center of IFSA, Shanghai Jiao Tong University, Shanghai* 200240, *China*
[8] *SUPA, Physics Department, University of Strathclyde, Glasgow G4 0NG, UK*

(Received 29 August 2016; revised manuscript received 23 September 2016; published online 25 October 2016)

The filamentation instability was observed in the interaction of two counter-streaming laser ablated plasma flows, which were supersonic, collisionless, and also closely relevant to astrophysical conditions. The plasma flows were created by irradiating a pair of oppositely standing plastic (CH) foils with 1ns-pulsed laser beams of total energy of 1.7 kJ in two laser spots. With characteristics diagnosed in experiments, the calculated features of Weibel-type filaments are in good agreement with measurements.

Keywords: Weibel instability, filamentation, laser plasma

PACS: 52.38.Fz, 52.35.Qz, 52.30.–q **DOI:** 10.1088/1674-1056/25/12/125201

1. Introduction

Shocks are ubiquitous high energy astrophysical scenarios in universal plasmas. Due to the fact that the spatial scales at which the plasma properties change are smaller than the particle–particle collision lengths, shocks observed usually around the supernova remnants are collisionless, i.e., it is the interactions of charged particles with local electromagnetic fields that helps stagnating particles and forming the shock structure. Collisionless shocks are expected to be capable of accelerating ultrahigh energy cosmic rays (UHECR) through the Fermi mechanism,[1] based on which one case of astronomic observations of UHECR[2] suggested that the magnetic field needed during the acceleration process is $\sim$ mGs (1 Gs $= 10^{-4}$ T), a thousand times of the background magnetic strength of μGs. However, the physical mechanisms of magnetic field generation and amplification that play important roles also in many other astrophysical phenomena are still attractive questions. One hypothesis for the shock structures is that the magnetic field is generated through Weibel Filamentation Instabilities (FI)[3,4] during interaction between outflow plasmas, reorganized and amplified, forming transverse structure (perpendicular to the plasma flow along the radial direction) at large scales and capturing/stagnating incident charged particles to form shocks within which they accelerate and irradiate the synchrotron emission, manifesting magnetic field configuration they are gyrating around.[5–7] But the opportunities to observe details of the collisionless shock behaviors are limited astronomically. The giant lasers, which can produce plasma flows with speeds of thousands of miles per seconds, approaching the observed speed of cosmic plasma jets, might help to pave the way to quantitatively inspect models of the astrophysical phenomena. As to the above hypothesis for collisionless shocks and ultrahigh energy cosmic rays from supernova, laboratory laser-plasma experiments designed for astrophysics study have to demonstrate, step-by-step, the magnetic field's generation and amplification, the density's stagnation and accumulation, and the charged particles' acceleration and gyration to radiate synchrotron emission.[7,8]

There are pioneering laboratory experimental works about the magnetic field generation through Weibel instabilities,[9–11] and some about collisionless shocks due to the electrostatic instabilities.[12] But the spontaneous magnetic field mediated collisionless shock, which is the right physical process closely underlying many astrophysical scenarios, still keeps lacking in laboratory experiments due to the limitations

*Project supported by the National Natural Science Foundation of China (Grant Nos. 11074297, 11674146, and 11220101002) and the National Basic Research Program of China (Grant No. 2013CBA01500.

†Corresponding author. E-mail: qldong@aphy.iphy.ac.cn

© 2016 Chinese Physical Society and IOP Publishing Ltd

inherited from the conflicts between the plasma speed and the small size of laser plasma systems, which reduces the possibility of the whole evolution of physical processes to finish. Long time expectations for similar type of experiments on the platform of the National Ignition Facility (NIF) of the USA, the largest lasers in the world, are not still matched, as NIF's configuration was designed originally for the indirectly driven fusion missions so that not many laser beams and energies can be utilized for the plasma flow production. If this is the case, NIF experiments on collisionless shocks and related physical processes are not expected to produce more than that on other giant laser platforms. In this situation that various giant laser platforms can provide plasma systems with different parameters and diagnostics with different capabilities, it is necessary to have more data so that information of the early time scenario can be collected as much as possible to inspect the hypothesis model.

This paper reports observations of the Weibel-type density filamentation of counter streaming laser plasmas, which act as the supplement for the magnetic filaments observed in Ref. [9]. With measured properties of the laser plasma flows, the calculated growth rates of the instability modes agree well with the features of the plasma filaments. The interaction between filaments was taken into consideration of the filamentation evolution at the nonlinear regime, giving the right transformation trend of the distribution of spaces between filaments. However the filamentation instability is still far from the saturation regime and the collisionless shock formation, indicating large laser energy and intensity are needed for the Weibel Instabilities mediated collisionless shock study.

2. Experimental setup

Experiments were conducted on the SG-II laser facility platform in September, 2011. The setup is shown in Fig. 1. Two face-to-face standing CH foil targets of 5 mm × 5 mm were used to generate a pair of counter-streaming plasma flows. To produce asymmetrical plasma flows, seven 1ns-pulsed laser beams were launched and divided into two groups: the 4 southern laser beams of 1 kJ were focused on the northern target, and the 3 northern of 0.7 kJ on the southern target. The southern bunch of laser beams was delayed by 1 ns making sure that two plasma flows have different properties when they encounter between two CH foils separated by 4.5 mm. The laser spots on CH foils were 150 μm in diameter, generating an average laser intensity of 10^{14} W/cm^2–10^{15} W/cm^2. The 9th laser beam of SG-II platform was used as a probe to measure the plasma density profile through Normaski Interferometry (NI) and shadowgraphy techniques with a magnification ratio of 1.5. With the probe of 2ω (527 nm in wavelength) and 30 ps duration was applied, the upper measurement limit of the electron density is around 5×10^{19} cm^{-3}–8×10^{19} cm^{-3} in our experiments. At different delay times with respect to the southern bunch, the recorded interferometry can provide the temporal evolution of the electron density. One interferometry image and one shadowgraphy image are given as examples, which are also the main objectives for our analysis. For all shots, x-ray pinhole cameras of 10-times magnification were also used to measure the uniformity of the laser spots. For comparison, a single plasma flow was produced by a pulsed laser with the same intensity. A flat-field spectrometer was used in this experiment for the soft x-ray emission line measurements from the position at the middle between the two CH foil targets with the view field width of 3 mm and the spatial resolution of 0.2 mm.The intensity ratio between lines was used to estimate the electron temperature and density by comparing calculated results from the FLYCHK[13] code and the measured ones.

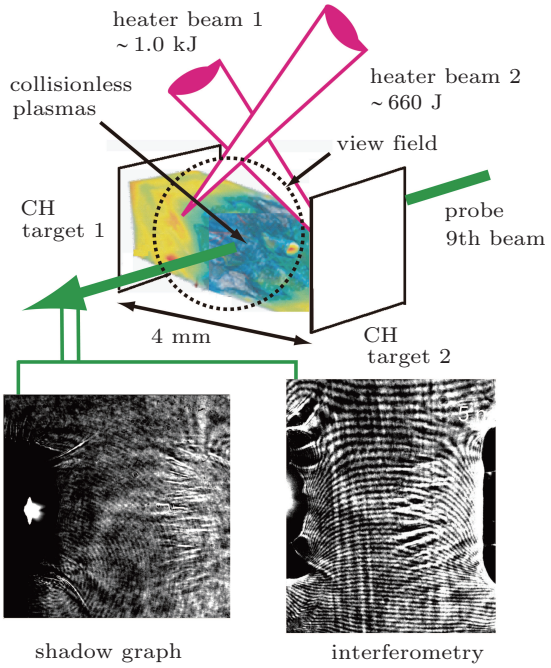


Fig. 1. (color online) Experimental setup. After passing through the sample plasma perpendicularly to the flow direction, the probe light was divided into two arms for the Normaski Interferomentry (NI) and the shadowgraphy techniques, respectively. Sample CCD pictures for the two kinds of diagnosis are given for the delay time of 4.5 ns.

3. Experimental result analysis

3.1. Plasma's electron temperature and density

Figure 2 shows the recorded soft x-ray emission spectra. The intensity ratio between He-like C^{4+} 22.7 nm and 24.9 nm was used to determine the electron temperature by comparing the measured value and the calculated one from the FLYCHK code. The electron temperature was estimated to be around 50 eV and the electron density around 4×10^{18}/cm^3, consistent with that from the interferometry image recorded at 2 ns (not shown in the context). It is noted that since the soft x-ray emission lines are time-integrated, the spectra should consist of emission lines from the time the plasma flow arrived at

the viewed position to the far end of the experiment, meaning that the estimated electron temperature should be lower than the highest value during the plasma evolution. As the plasma cools down, the intensity of lines from lower ionization states might dominate the spectra. But this did not affect the accuracy of the method to estimate the electron temperature since the intensity ratio utilized here were of emission lines from the same carbon ions, and the emission lines from lower ionization states locate at the spectral range of longer wavelengths.

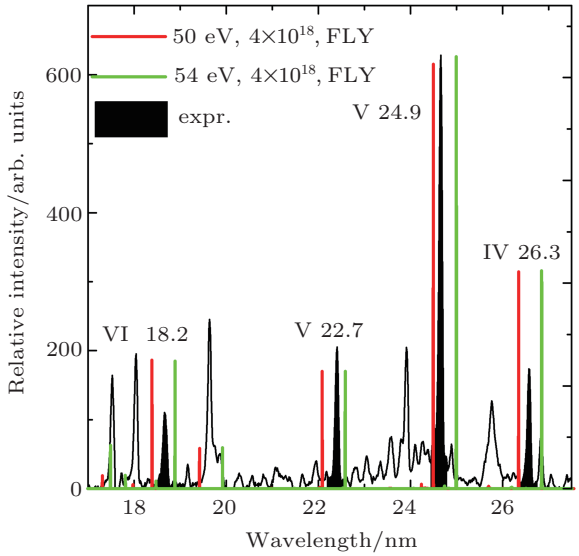


Fig. 2. (color online) Experimentally measured soft x-ray emission spectra of carbon ions are compared with the calculated ones by the FLYCHK code to give the electron density of $n_e \sim 4 \times 10^{18}$ cm^{-3} and the temperature $T_e \sim 50$ eV.

3.2. Characteristics of the filamentation behaviors

Figure 3(a) shows the recorded shadowgraph at the time delay of 4.5 ns. The main interesting feature is the filaments that follow the expansion direction of the plasma ball. The filament location near the side of the right (northern) laser spot rather than the center is attributed to 1-ns delay of the launch time of the Southern bunch of lasers. The shot time arrangement of, as well as the different energy contained in, two laser spots produced a condition with tenuous background plasma for the hotter plasma from the right target, while avoiding the Southern laser heating of the preformed plasma. The indicated over-dense plasma region shows the edge of plasma with density higher than 5×10^{19} cm^{-3}. To show the nature of the filament, the detailed distribution profile of several filaments were given in Fig. 3(b). As shown by the inset for the theoretical basis of the shadowgraphy technique, the black and white filament pairs were caused by the deflection of the probe light. The black part of the filament was produced when the corresponding part of the originally uniform probe was deflected by the nonlinear part of the electron density spatial distribution profile into the other part where the electron density was uniform or presented a linear spatial distribution. So, the filaments with black and white area pairs were actually edges of electron currents that were separated by the instability generated magnetic fields. The width of the electron current can be defined accordingly then. When inspecting the filaments closely, one found that the filaments can be divided into two groups according to their lengths. The longer filaments are supposed to be located in or parallel to face-on planes containing two laser spots, while shorter filaments are supposed to be the projections of those filaments with larger angles to face-on planes. Figure 3(d) gives the shadowgraph recorded at the time delay of 3.5 ns, which shows the beginning stage of the filamentation behavior. Only several filaments present at two different areas. Figure 3(c) shows the transverse profile of these filaments in the same area but recorded at time delays of 3.5 ns and 4.5 ns, respectively. The evolution of the filaments is clear as the width of the electron currents or the space between filaments changed from 90 μm–120 μm to 150 μm–400 μm.

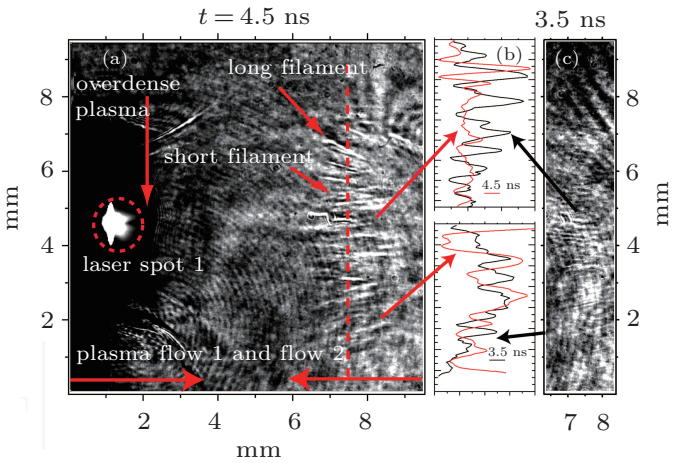


Fig. 3. (color online) Shadowgraphs taken at 3.5 ns (c) and 4.5 ns (a) delay times with respect to the tail of the Southern bunch of laser pulses. Panel (b) gives the transverse spatial distribution profile of filaments at the arrow-marked positions but at 3.5 ns and 4.5 ns, respectively. The spaces between the filaments were found to grow from 90 μm–120 μm at 3.5 ns to 150 μm–400 μm at 4.5 ns.

The profile of the filament distribution is analyzed by using different band FFT (Fast Fourier Transformation) filters, as shown in Fig. 4. In Fig. 4(a), the red line presents the filtered profile involving all (short and long) filaments spaced by 90 μm–250 μm, while the blue line presents only long filaments spaced by 400 μm–600 μm as indicated by the solid triangles. Both FFT-filtered distributions reproduce the corresponding peaks or the filaments in the experimental profile. One explanation for the experimental observation is that the spaces between real filaments in three dimensions is 400 μm–600 μm, and the smaller value of 90 μm–250 μm is due to the "forest-effect" of the projection process. Another explanation is more possible that the two correlation scales are produced from the filament coalescence processes as will be shown in the next section. The frequency distribution from the FFT analysis is shown in Fig. 4(b), which confirms the dominance of the larger filament space or the electron current width.

For the real size of the experimental filaments, the magnification ratio should be eliminated by dividing the above measurements with 1.5.

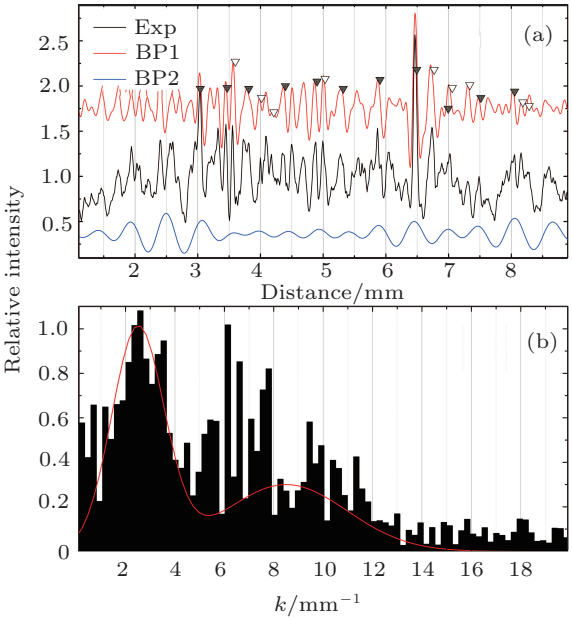


Fig. 4. (color online) (a) The spatial distribution of filaments along the dashed line in Fig. 3(a). The black line is the experimental result. With different band FFT (Fast Fourier Transformation) filters, the red line presents all (short and long) filaments spaced by 90 μm–250 μm, while the blue line presents only long filaments spaced by 400 μm–600 μm as indicated by the solid triangles. (b) The FFT spectrum of the spatial distribution of filaments. It is noted that after eliminating the instrumental magnification effects, the real electron current widths or the spaces between all and only long filaments are around 120 μm and 260 μm, respectively.

To explore the mechanisms underlying the filamentation, growth rates were calculated for various instabilities with the diagnosed plasma parameters. It is found that for the filamentation parallel to the flow velocity, the Weibel Instability is the most likely mechanism. The dispersion relation of the beam-Weibel instability is given by[14]

$$\omega^2 = (kc)^2 - \sum \omega_{ps}^2 \left[\frac{v_{\mathrm{ths}}^2 + 2(V_{\mathrm{s}} \sin(\theta)^2)}{v_{\mathrm{ths}}} (1 + \zeta_{\mathrm{s}} Z(\zeta_{\mathrm{s}})) - 1 \right],$$

where

$$Z(\zeta_{\mathrm{s}}) = \pi^{-1/2} \int_{-\infty}^{\infty} \frac{\mathrm{e}^{-z^2}}{z - \zeta_{\mathrm{s}}} \mathrm{d}z$$

is the dispersion function,

$$\zeta_{\mathrm{s}} = \zeta_{\mathrm{s}}(\omega, k, \theta) = (\omega/k - V_{\mathrm{s}} \cos(\theta))/v_{\mathrm{ths}},$$

with V_{s} the bulk velocity, and $v_{\mathrm{ths}} = \sqrt{(2T/m)}$ is the average thermal velocity at temperature T. The calculation result is shown in Fig. 5, indicating the Weibel instability grew at $\Gamma \sim 10^{-4} \omega_{\mathrm{pe}}$, which means, for plasmas with the electron density of 4×10^{18} cm^{-3}–5×10^{18} cm^{-3} that were measured by the interferometry technique and from the soft x-ray emission spectra, the space between filaments is around 90 μm, agreeing well with the measurements when the filamentation behavior appeared at the time delay of 3.5 ns. With the calculated growth rate, the amplitude of the magnetic field around filamentations will grow by hundreds of times in several nanoseconds if the approximation $B/B_0 \sim \exp(\Gamma t)$, making it observable.

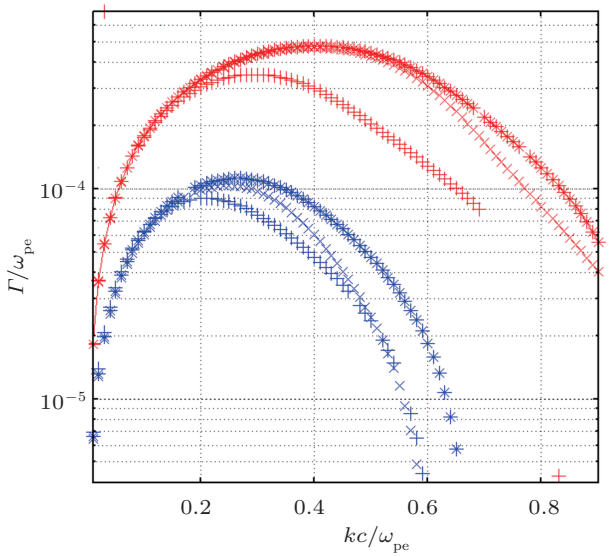


Fig. 5. (color online) Growth rate Γ of filamentations parallel to plasma bulk velocity V_{s}. Effects of the plasma–ion–beam interaction (+), the plasma–electron–beam (×), and the plasma–plasma interaction Γ (∗) were compared. The upper group data represent for the plasma–plasma interaction with $V_{\mathrm{s}} = 1000$ km/s, while the lower group for the interaction with $V_{\mathrm{s}} = 650$ km/s.

Contributions to growth rates from different plasma properties were also studied. As CH plasma contains various carbon ions, to simplify the calculation $C^{(4+)}$ and H^+ were adopted. Growth rates of the following cases were calculated: plasma–plasma interactions, plasma–ion–beam interaction, and plasma–electron–beam interaction. The growth rates changed little for three different cases with the same bulk velocity. But for higher bulk velocity, the growth rate increased significantly. The growth rate for the bulk velocity of $V_{\mathrm{s}} = 1000$ km/s is nearly one order of magnitude larger than that with $V_{\mathrm{s}} = 500$ km/s.

3.3. The temporal evolution of the filamentation instability

The study of the evolution of the Weibel instability filaments is of importance that it helps to design further laser plasma experiments closely related to the astrophysical collisionless shock, the suggested origin of ultra high energy cosmic rays. It is noted that the Weibel instability is a nonresonant electromagnetic hydrodynamical instability with modes of a broadband wavelength excited simultaneously but at different growth rates. The mode with the largest growth rate usually presents on the spatial scale of the basic Langmuir fluctuation of plasmas, grows and saturates rapidly but at a lower amplitude. Those modes with larger scales continue growing and saturate at larger amplitudes. However, the observed fluctuation scale or wavelength in the experiments increased with the time and could not be simply attributed to the corresponding mode growth. The dispersion relation shows the

possibility for what kind of modes are capable of being excited and growing under the present experimental conditions, the magnetic interaction between filaments however helps to determine the evolution of the space between filaments or the width of the electron currents. The interaction process plays dominant roles especially after the corresponding modes saturate as the filaments will merge when they approach each other closely enough, and form new wider filaments that are allowed by the dispersion relation. Actually, for the filament distribution to evolve, contributions are from both of the above two processes simultaneously.

By pre setting filament current without any physical scenarios specified, and taking considerations only of the mutual magnetic interaction between filaments, Medvedev *et al.*[15] designed a toy model to investigate the filament coalescence behavior in a nonrelativistic plasma system, and gave the time-dependence of the correlation lengths as $\lambda_{\mathrm{WI,M}}(t) = D_0\sqrt{2^{t/\tau_{\mathrm{NR}}}}$. Here, D_0 was defined as the initial diameter of the filament current and $d_0 = 2D_0$ as the initial separation between filaments

$$\tau_{\mathrm{NR,M}} = \sqrt{\pi\mu_0}cD_0/I_0 \cdot \mathrm{erfc}(\sqrt{\ln 2}) = \sqrt{4\pi}\omega_{\mathrm{pi}}^{-1}\frac{c}{V_{\mathrm{s}}} \cdot \mathrm{erfc}(\sqrt{\ln 2})$$

with $\mu_0 = m_{\mathrm{en}}(\pi D_0^2/4)$ being the mass per unit length, and $I_0 = Z_{\mathrm{i}}enV_{\mathrm{s}}\pi D_0^2/4$ the filament current. The initial separation was set as the smallest correlation length for the mode allowed by the dispersion relation, $d_0 \sim c/\omega_{\mathrm{pe}}$.

To compare with the experimental results, it is necessary to include effects of the growth and saturation of the allowed modes. However, self-consistent studies of filamentation dynamics are still lacking along with the self-consistent analytical theory describing the saturation behavior of the Weibel instability. Ruyer *et al.*[16] provided an analytical model for the Weibel filamentation instability by combining the quasilinear model and the coalescence behavior at post saturation stage. The model gives an expression of the typical coalescence time, $\tau_{\mathrm{NR,R}}$, that has a similar dependence on ω_{pi} as in Medvedev's model, indicating that the model's inclusion of the coalescence behavior only during the post saturation stage is equivalent to the preset of filament current properties. We would like to invoke Ruyer's analytical expression for the long-term evolution of the electron current widths, since the asymptotic resolution is not affected by the details of the evolution process, i.e.,

$$\lambda_{\mathrm{WI,R}}(t) = 2\pi/k \sim \frac{(V_{\mathrm{s}}/c)^2}{12\pi^2\sqrt{2\alpha_{\mathrm{i}}}}\frac{c}{\omega_{\mathrm{pe}}}(\omega_{\mathrm{pi}}t)^2.$$

The correlation length increased with t^{α} with $\alpha = 2$ here in the Ruyer's model describing the Weibel instability in nonrelativistic plasmas. It is worth noting that in the relativistic regime, the dependence of the filament width on time is linear.[15,17]

The experimental observation of the filament width at delay times of 3.5 ns, 4.5 ns, and 6.5 ns are co-plotted in Fig. 6 with the above theoretical curves. The two data points of $t = 4.5$ ns present for the two correlation length scales from Fig. 4. The trend of the experimental results matches the theoretical curves qualitatively, but with big deviations from both theoretical curves. More likely, if only the dominant filaments of larger scales at 4.5 ns are taken into considerations, the experimental data seems to follow a linear increase with time, although the present experiment has a Lorentz factor $\gamma \sim 1$ and is still far from a relativistic regime. Several data points and the limits in the spatial resolution and the observable density fluctuation in the experiments might not help to determine which model is more accurate. The other possibility that prevents the above models from accurately predicting the experimental results are the over-simplified description of the filament coalescence process. For example, both models omit the roles of newly formed filaments that might have smaller separation distance to other existing filaments and between themselves.

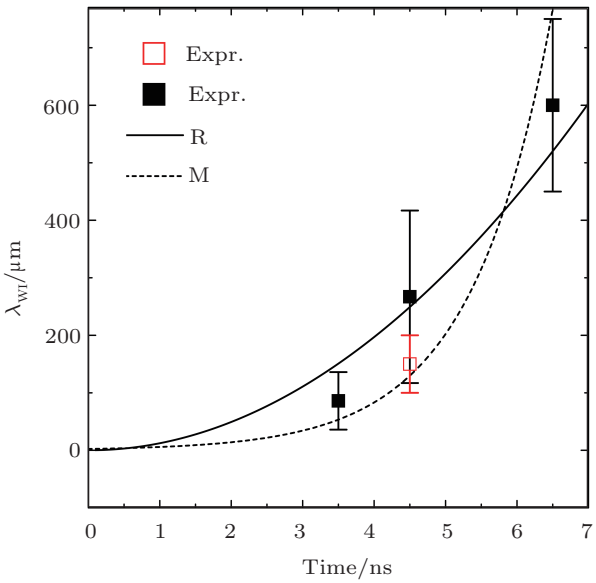


Fig. 6. (color online) The temporal evolution of the current filament widths. Scattered symbols are experimental data with the error bar showing the width range. The solid line is from Medvedev's model, and the dashed line from Ruyer's model. For the time delay at 4.5 ns, two data points represent the two correlation scales derived from Fig. 4(b).

4. Summary

A pair of counter-streaming laser plasma systems were found to have filamentation behaviors which were attributed to the Weibel instability. The characteristics of the filamentation were analyzed with the Fast Fourier Transform method, and compared to the numerical results calculated from the dispersion relation by using the experimental plasma properties. However, the magnetic field generated through the instability is still weak, far from the strength needed for stagnating charged particles to form collisionless shocks as observed in

SN remnants. The evolution of the separation distances between Weibel instability filaments were also studied. The comparison between the experimental measurements and results from simplified models indicates that in the future experiments, it is necessary to have a larger plasma system with lower mass density so that the Weibel instability is allowed a longer time to grow into a nonlinear regime, and the larger filament width allows the density fluctuation measurements to be more accurate.

Acknowledgment

We thank all staff of the National Laboratory of High Power Lasers and Physics, and the target manufacture group of the Research Center of Laser Fusion, Chinese Academy of Engineering Physics for much help.

References

[1] Fermi E 1949 *Phys. Rev.* **75** 1169
[2] Yasunobu U, Felix A A, Takaaki T, Tadayuki T and Yoshitomo M 2007 *Nature* **449** 576
[3] Weibel E S 1959 *Phys. Rev. Lett.* **2** 83
[4] Fried B D 1959 *Phys. Fluids* **2** 337
[5] Cassam-Chena G, Hughes J P, Reynoso E M, Badenes C and Moffett D 2008 *Astrophys. J.* **680** 1180
[6] Suzuki-Vidal F 2015 *Nat. Phys.* **11** 98
[7] Takabe H, Kato T N, Sakawa Y, *et al.* 2008 *Plasma Phys. Control. Fusion* **50** 124057
[8] Drake R P and Gregori G 2012 *Astrophys. J.* **749** 171
[9] Fox W, Fiksel G, Bhattacharjee A, Chang P Y, Germaschewski K, Hu S X and Nilson P M 2013 *Phys. Rev. Lett.* **111** 225002
[10] Quinn K, Romagnani L, Ramakrishna B, *et al.* 2012 *Phys. Rev. Lett.* **108** 135001
[11] Huntington, Fiuza F and Ross J S, *et al.* 2015 *Nat. Phys.* **11** 173
[12] Kuramitsu Y, Sakawa Y, Morita T, Gregory C D, Waugh J N, Dono S, Aoki H, Tanji H, Koenig M, Woolsey N and Takabe H 2011 *Phys. Rev. Lett.* **106** 175002
[13] Lee R W and Larsen J T 1996 *J. Quantum Spectrsc. Radiat. Transfer* **56** 535
[14] Tautz R C and Schlicheiser R 2006 *Phys. Plasmas* **13** 062901
[15] Medvedev M V, Fiore M, Fonseca R A, Silva L O and Mori W B 2005 *Astrophys. J.* **618** L75
[16] Ruyer C, Gremillet L, Debayle A and Bonnaud G 2015 *Phys. Plasmas* **22** 032102
[17] Gedalin M, Medvedev M, Spitkovsky A, Krasnoselskikh V, Balikhin M, Vaivads A and Perri S 2010 *Phys. Plasmas* **17** 032108